Journal of the European Ceramic Society 22 (2002) 49–59

www.elsevier.com/locate/jeurceramsoc

Defect chemistry and electrical characteristics of undoped and Mn-doped ZnO

Jiaping Han, P.Q. Mantas, A.M.R. Senos *

Department of Ceramic and Glass Engineering/UIMC, University of Aveiro, 3810-193 Aveiro, Portugal

Received 30 October 2000; accepted 16 February 2001

Abstract

Undoped and Mn-doped ZnO samples were sintered at 1373, 1473, and 1573 K, for 2 h, in air, and then quenched to room temperature. Defect concentrations in these samples at the sintering temperatures and at room temperature and below were calculated using a refined defect model. Using the calculated electron concentrations and assuming a constant electron mobility of 100 cm^2/Vs, conductivities at room temperature were calculated and compared with experimental ones. The agreement between the experimental and calculated conductivities is very good for all the samples of undoped and Mn-doped ZnO. In the Mn-doped ZnO case, the ionisation energy of the Mn defect in ZnO was estimated to be ~2.0 eV. Using the experimental conductivities and the calculated electron concentrations, the electron mobilities were calculated between 70 and 300 K. The results show that the temperature dependence of the mobility in undoped ZnO is similar to that in ZnO single crystals observed in other works, and heavy Mn doping significantly reduces the electron mobility below room temperature probably due to impurity scattering. The role of Mn on the electrical conductivity of ZnO could be understood.

Keywords: Defects; Electrical conductivity; Sintering; ZnO

1. Introduction

Zinc oxide founds a wide range of scientific and technological applications, such as varistors,[1] gas sensors,[2] or in the form of film, being applied as piezoelectric transducers,[3] planar optical waveguides,[4] and transparent electrodes.[5] These applications directly depend on the defect chemistry of ZnO. In ZnO based varistors, for example, the nonlinear current-voltage characteristic caused by potential barriers at the grain boundaries, is influenced by changes in the defect chemistry occurring during the cooling period.[6–9] These changes arise from both the bulk of the grains and the grain boundaries, and are due to different ionisation energies of the actual defects, either in high concentration frozen in the bulk of the materials, or in low concentration at grain boundaries where they were annihilated during cooling. In order to understand and to obtain excellent electrical properties of ZnO, it is important to investigate the defect chemistry of this material.

* Corresponding author. Tel.: +351-234-370257; fax: +351-234-25300.

E-mail address: anamor@cv.ua.pt (A.M.R. Senos).

It is known that sintered ZnO is a semiconductor at room temperature, exhibiting an *n*-type electrical conductivity under normal zinc and oxygen partial pressures, which is due to an excess of the metal. This zinc excess gives origin to intrinsic donors in ZnO, which can be assigned either to the interstitial zinc (Frenkel defect),[10–12] or to the oxygen vacancy (Schottky defect).[13–15] These two types of defects have similar electrical properties, therefore being difficult to distinguish between them experimentally. In addition, some of the ionisation energies of the intrinsic defects and some of the equilibrium constants for the defect reactions in ZnO have not yet been completely identified. One of the main purposes of this work is to derive a model for the defect equilibria in undoped ZnO, which can account for the experimentally observed electrical conductivity in the material at different temperatures.

Another important point to address in this paper is to understand the effect of manganese addition to ZnO. In previous works,[16,17] we studied the effect of Mn-doping on the densification and grain growth of ZnO ceramics, and found that Mn-doping reduces the densification rate of ZnO in the early stage of sintering,[16] while in the intermediate and final stages of sintering promotes the

0955-2219/01/$ - see front matter
PII: S0955-2219(01)00241-2

grain growth of ZnO.[17] It is also known that this dopant improves the non-linear behaviour of ZnO based varistors,[18] which was connected to its presence at grain boundaries. However, its role with respect to the defect chemistry of ZnO is not known. In the present work, samples were quenched from the sintering temperature down to room temperature. With this procedure, we tried to eliminate the possible effect of ion migration to the grain boundaries,[9] or the reaction of grain boundary defects with ambient oxygen,[7,19] on the electrical conductivity of the samples. Therefore, the results should express the role of manganese in the ZnO bulk, if the solubility limit of this dopant in the ZnO material was not exceeded at the sintering temperature.

2. Experimental procedure

Reagent grade ZnO powders (Aldrich, Milwaukee, WI) with 99.9% purity and mean particle size of 0.26 μm was used. To dope with Mn, alcohol solutions of hydrated manganese nitrate [$Mn(NO_3)_2$. $4H_2O$] were prepared and mixed with ZnO powder in a planetary milling for 4 h using a plastic container without balls. The amount of manganese ranged from 0.1 to 0.6 mol%. The slurry was dried at 353 K, and the obtained powder was calcined at 723 K for 1 h. Disk-shaped specimens of 10 mm diameter and 1–2 mm height were obtained by uniaxial pressing at 100 MPa, followed by isostatic pressing at 200 MPa.

The temperature of a tubular furnace was raised up to a predetermined value (1373, 1473, and 1573 K). Samples were quickly inserted in the centre of the furnace. Appropriate corrections were made for the equilibration time, so that the heat treatment of the individual samples may be considered isothermal. After sintering for 2 h, the samples were quenched to room temperature in air.

Trace elements in the sintered samples were analysed by inductively coupled plasma (ICP) emission spectroscopy, as shown in Table 1. The relative densities of fired specimens were determined by the Hg-immersion method, using 5.67 g/cm^3 as the ZnO theoretical density. The relative densities of all the samples are in the range of 92–96%.

Specimens for electrical measurement were polished with 1200-grit SiC on both sides, and ultrasonically cleaned. Gold electrodes were sputtered over the sample faces, and In–Ga electrodes were also used to check the type of the produced contacts. Electrical conductivity and electrical current-voltage behaviour were measured with an electrometer (Model 617, Keithley, USA), a current source (Model 220, Keithley, USA) and a multimeter (Model 197, Keithley, USA). Low temperature measurements were performed in a cryogenic system (Model HC-2, APD Cryogenics Inc., USA). Temperature control and measurements were performed with a calibrated silicon diode and a microprocessor cryogenic temperature controller (Model 9650, Scientific Instruments Inc., USA). All data were reproducible within the experimental error.

Table 1
Trace element analysis by inductively coupled plasma emission spectroscopy in sintered samples (data in atomic ppm)

Sample	Mn	Bi	Ba	Sr	Ca	Pb	Fe	Cu	Al	Na
Undoped	2.0	<2.1	<0.7	<0.7	<9.0	<7.0	<1.8	<1.8	<3.7	<13
0.1% Mn	928	<2.2	<0.7	<0.7	<3.9	<3.3	<1.3	<1.2	<4.2	<13
0.3% Mn	2701	<5.0	<0.4	<0.4	<6.5	<3.3	<3.1	<2.7	<9.7	<15
0.6% Mn	5088	<5.1	<0.5	<0.5	<4.9	<3.6	<3.4	<2.9	<11	<16

3. Results and discussion

The electrical conductivity of ZnO at room temperature is controlled by the intrinsic defects generated at high temperature and by the presence of dopants, either specifically added to the materials or not. During the cooling of the samples, the defects tend to migrate to the grain boundaries to be annihilated (intrinsic defects) or to be exsolved, if their solubility limit is attained (extrinsic effects). This migration process is normally slow and its kinetic is thermally activated, meaning that at some temperatures not much lower than the sintering one, only the defects near the grain boundaries are effectively eliminated. The resulting concentration profiles considerably affect the room temperature electrical properties of ZnO. In order to avoid this process, samples were quenched from the sintering temperature. On doing this, we can assume that at room temperature the defects are homogeneously distributed in the material, and that their concentrations are the same as those at the sintering temperature, except for electrons and holes which can readily diffuse at room temperature. Therefore, knowing the equilibrium constants for the defect reactions at the sintering temperature, the concentration of the defects at room temperature and the density of carriers in the conduction band, n, can easily be calculated. From this value, the calculated conductivity, $\sigma_{cal} = n\mu e$, can be compared with the experimental one, σ_{exp}, provided that the carriers mobility, μ, is known.

Fig. 1 shows the room temperature dc electrical conductivity of the sintered samples as a function of the Mn content in the samples, for the different sintering temperatures. It can be seen that the higher the Mn content, the lower the conductivity of the samples, and the higher the sintering temperature, the higher the conductivity. Both observations are consistent with previous results from other works,[14,15] and the second observation is also consistent with the general rule that the higher the sintering temperature, the higher the concentration of native defects, namely the intrinsic donor defects. The

effect of Mn is not clear at the moment, because it is normally reported that Mn is a deep donor in ZnO,[15,18,20–22] and consequently one might expect that it plays no particular role in the ZnO conductivity at room temperature. Besides, we have no information about the influence of Mn on the mobility of the carriers, and there is also the possibility that the presence of Mn at the grain-boundaries may promote the appearance of electrical barriers.[19,23]

Fig. 2 shows the electrical current density (J)-electric field (E) curves of the undoped and Mn–doped samples at room temperature. These curves do not depend on the type of electrodes used (gold or In–Ga alloy), and it is clear that, at least up to 0.1 A/cm^2 or 1500 V/cm, no non-linear behaviour was observed (although not shown, the same is true for the undoped samples). This observation allows us to state that Mn is not playing any particular role in grain boundaries, and in order to simplify the following calculations we shall assume that Mn is homogeneously distributed throughout the material. The decrease of the conductivity upon the Mn addition is not related to electrical barriers built up at grain boundaries due to the presence of Mn, but instead to a decrease of the carriers density and/or a decrease of the carriers mobility in the bulk.

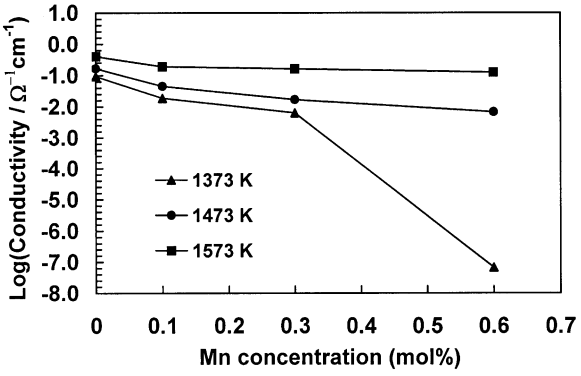

Fig. 1. Experimental conductivities at 300 K of undoped and Mn-doped ZnO, quenched after sintering at 1373, 1473 and 1573 K, respectively.

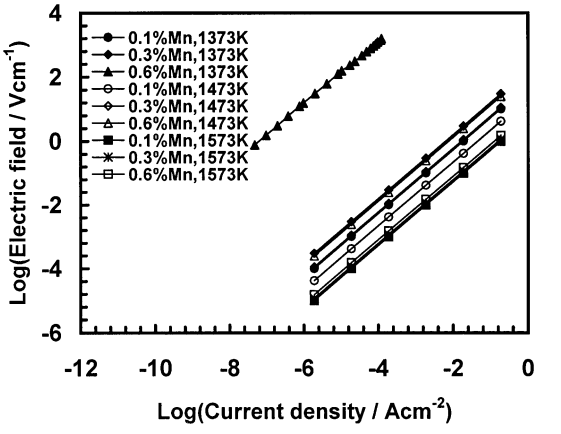

Fig. 2. Electrical current density (J)-electric field (E) characteristics for Mn-doped ZnO at room temperature.

Table 1 shows the impurity levels in the materials. It can be observed that each background impurity of Bi, Ba, Sr, Ca, Pb, Fe, Cu, Al and Na, is much smaller than the Mn doping level in sintered samples. The level of Na is almost constant, and this is an element that could act as an acceptor,[24] thus promoting a decrease of the conductivity. Some particular care should be put on the Al content, because it is known that 10 ppm of Al is enough to control the carrier density in ZnO.[23] The 0.3 and 0.6 mol% Mn doped samples have an Al content around 10 ppm, and they should show a high conductivity. That is not the case (see Fig. 1), but we can not rule out its influence on the electrical properties before having a picture of the true role of Al in these samples. Table 1 also shows that the final amount of the Mn in the samples is less than 10∼15% of the initial value. This probably comes from the drying process. In what follows, we will take the actual content of Mn in the samples as shown in Table 1, although we keep the samples identification as 0.1, 0.3 and 0.6 mol%.

Our first task is now to draw a model for the ZnO defect chemistry that allows us to explain the results of Fig. 1. For a first approach we will assume a carrier mobility of 100 cm^2/Vs,[25] for room temperature, whatever the sintering temperature of the sample or its chemical composition. With this value, we can then compare the calculated conductivities with the experimental ones, and therefore to check the reliability of the model. The second task will deal with the electrical properties at temperatures below room temperature.

3.1. Defect chemistry and room temperature conductivity

To calculate the room temperature conductivity, besides the carrier mobility, we need to know the carrier density. Since ZnO is a n-type semiconductor at room temperature, we will neglect the contribution of the hole conductivity if $p \leqslant 10^{-3}n$ (p being the hole concentration in the valence band, and n the electron concentration in the conduction band). One only needs to know n and p at room temperature, and these come from the ionisation of donors, acceptors, and the creation of electron-hole pairs. To do this, we must know the concentration and energy position of each defect, and the band gap energy at room temperature. Since we quenched the samples from the sintering temperature, it can be considered that the total concentration of any ionic defect is frozen, i.e., the total ionic defect concentration is constant whatever the temperature well below the sintering one. For example, the total zinc interstitial concentration, $[Zn_i]_{Total}$, at the sintering temperature will be the same as at room temperature, and it is equal to (mass action)

$$[Zn_i]_{Total} = [Zn_i^{\times}] + [Zn_i^{\bullet}] + [Zn_i^{\bullet\bullet}] \quad (1)$$

where we have adopted the Kröger–Vink's notation for the defects: $Zn_i^{\times}$ for the neutral defect, $Zn_i^{\bullet}$ for the monoionised defect, and $Zn_i^{\bullet\bullet}$ for the full ionisation. In this equation, and also in those equivalent for the other defects, only the concentrations of $Zn_i^{\times}$, $Zn_i^{\bullet}$, and $Zn_i^{\bullet\bullet}$, change with temperature. Therefore, we need to know the total concentration of each defect at the sintering temperature, and then we can compute their ionised concentrations at room temperature in order to calculate the conductivities. This type of calculation was previously reported by others,[10,12,14,15] and the key point is to have the equilibrium constants for the defects reactions.

Our analysis begins with the definition of the high temperature equilibria. Tables 2 and 3 show the values for the equilibrium constants at high temperature given by different authors. In Kröger's model,[13] the author proposes that the predominant donor defect in ZnO is the oxygen vacancy, V_O, while Hagemark[10] and Sukker and Tuller[12] propose that it is the zinc interstitial, Zn_i. This is the most controversial issue in the ZnO defect chemistry, because both defects give very similar electrical properties and it is difficult to distinguish them experimentally. The zinc interstitials come from the Frenkel reaction (K_F) in the Zn sublattice,

$$Zn_{Zn} \iff Zn_i^{\times} + V_{Zn}^{\times} \quad (2)$$

while the oxygen vacancy comes from the Schottky reaction (Ks),

$$0 \iff V_{Zn}^{\times} + V_O^{\times} \quad (3)$$

Our experimental work is limited to a temperature $\leqslant$1573 K, where Frenkel defects predominate, $K_F > K_S$, and the Schottky defects become increasingly important for higher temperatures[12] (see also data in Tables 2 and 3). On studying the sintering behaviour of pure ZnO, Senos[26] arrived at the conclusion that the results are better fitted with the assumption that the zinc interstitials are the predominant defects in ZnO, in this temperature

Table 2
Defect chemical reactions and related constants for ZnO in the Kröger's and Hagemark's models[a]

Reaction	Constant	Kröger's model	Hagemark's model[h]
$ZnO \iff Zn(g) + 1/2\ O_2(g)$	$K_{ZnO} = p_{Zn}p_{O2}^{1/2}$[b]	$1.50\times10^{10}\exp(-4.89/kT)$ ($atm^{3/2}$)	$1.50\times10^{10}\exp(-4.89/kT)$
$1/2O_2 \iff O_O + V_{Zn}^{\times}$	$K_O = [V_{Zn}^{\times}]p_{O2}^{-1/2}$	$1.29\times10^{23}\exp(-2.0/kT)(atm^{-1/2}cm^{-3})$	$8.87\times10^{19}\exp(-1.86/kT)$
$ZnO \iff Zn_i^{\times} + 1/2\ O_2(g)$	$K_R = [Zn_i^{\times}]p_{O2}^{1/2}$	$3.36\times10^{25}\exp(-4.76/kT)(atm^{1/2}cm^{-3})$	$1.56\times10^{29}\exp(-5.57/kT)$
$Zn_{Zn} \iff Zn_i^{\times} + V_{Zn}^{\times}$	$K_F = K_O K_R$	$4.33\times10^{48}\exp(-6.76/kT)$ (cm^{-6})	$1.38\times10^{49}\exp(-7.43/kT)$
$O_O^{\times} \iff V_O^{\times} + 1/2\ O_2(g)$	$K_{O2} = [V_O^{\times}]p_{O2}^{1/2}$	$3.87\times10^{30}\exp(-4.29/kT)(atm^{1/2}cm^{-3})$	–
$Nil \iff V_{Zn}^{\times} + V_O^{\times}$	$K_S = K_O K_{O2}$	$4.99\times10^{53}\exp(-6.29/kT)$ (cm^{-6})	–
$Zn_i^{\times} \iff Zn_i^{\bullet} + e'$	$K_1 = [Zn_i^{\bullet}]n/[Zn_i^{\times}]$[c]	–	$2N_C\exp(-0.05/kT)$ (cm^{-3})
$Zn_i^{\bullet} \iff Zn_i^{\bullet\bullet} + e'$	$K_2 = [Zn_i^{\bullet\bullet}]n/[Zn_i^{\bullet}]$	–	$1/2\ N_C\exp(-0.15/kT)$ (cm^{-3})
$V_O^{\times} \iff V_O^{\bullet} + e'$	$K_3 = [V_O^{\bullet}]n/[V_O^{\times}]$	$2N_C\exp(-0.05/kT)$ (cm^{-3})[f]	–
$V_O^{\bullet} \iff V_O^{\bullet\bullet} + e'$	$K_4 = [V_O^{\bullet\bullet}]n/[V_O^{\bullet}]$	$1/2\ N_C\exp(-2.0/kT)$ (cm^{-3})	–
$V_{Zn}^{\times} \iff V_{Zn}' + h^{\bullet}$	$K_5 = [V_{Zn}']p/[V_{Zn}^{\times}]$	$2N_V\exp(-0.8/kT)$ (cm^{-3})[f]	$2N_V\exp(-0.8/kT)$
$V_{Zn}' \iff V_{Zn}'' + h^{\bullet}$	$K_6 = [V_{Zn}'']p/[V_{Zn}']$	$1/2\ N_V\exp(-2.8/kT)$ (cm^{-3})	$1/2\ N_V\exp(-2.8/kT)$
$Nil \iff e' + h^{\bullet}$	$K_i = np$	$N_C N_V\exp(-E_g/kT)$ (cm^{-6})	$N_C N_V\exp(-E_g/kT)$
	m_e*[d]	$0.2m_0$ (kg)[e]	$0.3m_0$
	m_h*	$1.0m_0$ (kg)	$1.8m_0$
	$N_C = 2(2\pi m_e^* k/h^2)^{3/2}T^{3/2}$[g]	$1.92\times10^{15}T^{3/2}(cm^{-3})$	$7.94\times10^{14}T^{3/2}$
	$N_V = 2(2\pi m_h^* k/h^2)^{3/2}T^{3/2}$	$4.84\times10^{15}T^{3/2}(cm^{-3})$	$1.16\times10^{16}T^{3/2}$
	$E_g = E_g(0) - \beta_g T$	$3.1 - 10\times10^{-4}T$ (eV)[g]	$3.34 - 8\times10^{-4}T$

[a] For the defects, Kröger–Vink's notation is used.
[b] p_{O2} and p_{Zn} are the oxygen and zinc partial pressures.
[c] n and p are the electron and hole concentrations.
[d] m_e* and m_h* are the electron and hole effective masses
[e] m_0 is the free electron mass.
[f] N_C and N_V are the conduction and valence band density of states.
[g] E_g is the band gap energy, and k and h are the Boltzman and Planck constants, respectively.
[h] Note that the units of the constants in Hagemark's model are the same as those in Kröger's model and, therefore, are omitted.

Table 3
Defect chemical reactions and related constants for ZnO in the Sukker and Tuller's model and in the modified one used in the present calculations[a]

Reaction	Constant	Sukker and Tuller's model[i]	Present work
$ZnO \Longleftrightarrow Zn(g) + 1/2\ O_2(g)$	$K_{ZnO} = p_{Zn} p_{O2}^{1/2}$[b]	$1.50\times10^{10}\exp(-4.89/kT)$	$1.50\times10^{10}\exp(-4.89/kT)$
$1/2O_2 \Longleftrightarrow O_O + V_{Zn}^{\times}$	$K_O = [V_{Zn}^{\times}] p_{O2}^{-1/2}$	$1.2\times10^{17}\exp(-1.9/kT)$	$1.15\times10^{16}\exp(-1.86/kT)$
$ZnO \Longleftrightarrow Zn_i^{\times} + 1/2\ O_2(g)$	$K_R = [Zn_i^{\times}] p_{O2}^{1/2}$	$1.6\times10^{28}\exp(-5.57/kT)$	$1.56\times10^{29}\exp(-5.57/kT)$
$Zn_{Zn} \Longleftrightarrow Zn_i^{\times} + V_{Zn}^{\times}$	$K_F = K_O K_R$	$1.8\times10^{45}\exp(-7.47/kT)$	$1.8\times10^{45}\exp(-7.43/kT)$
$O_O^{\times} \Longleftrightarrow V_O^{\times} + 1/2\ O_2(g)$	$K_{O2} = [V_O^{\times}] p_{O2}^{1/2}$	–	–
$Nil \Longleftrightarrow V_{Zn}^{\times} + V_O^{\times}$	$K_S = K_O K_{O2}$	–	–
$Zn_i^{\times} \Longleftrightarrow Zn_i^{\bullet} + e'$	$K_1 = [Zn_i^{\bullet}] n / [Zn_i^{\times}]$	$1/2\ N_C\exp(-0.05/kT)$	$1/2\ N_C\exp[-(0.052-5.5\times10^{-6}T)/kT]$
$Zn_i^{\bullet} \Longleftrightarrow Zn_i^{\bullet\bullet} + e'$	$K_2 = [Zn_i^{\bullet\bullet}] n / [Zn_i^{\bullet}]$[c]	$2N_C\exp(-0.20/kT)$	$2N_C\exp[-(0.207-2.2\times10^{-5}T)/kT]$
$V_O^{\times} \Longleftrightarrow V_O^{\bullet} + e'$	$K_3 = [V_O^{\bullet}] n / [V_O^{\bullet}]$	$1/2\ N_C\exp(-0.50/kT)$[f]	$1/2\ N_C\exp[-(0.331-3.5\times10^{-5}T)/kT]$
$V_O^{\bullet} \Longleftrightarrow V_O^{\bullet\bullet} + e'$	$K_4 = [V_O^{\bullet\bullet}] n / [V_O^{\bullet}]$	$2N_C\exp(-2.0/kT)$	$2N_C\exp[-(2.066-2.2\times10^{-4}T)/kT]$
$V_{Zn}^{\times} \Longleftrightarrow V_{Zn}' + h^{\bullet}$	$K_5 = [V_{Zn}'] p / [V_{Zn}^{\times}]$	$1/2\ N_V\exp[-(0.9\sim1.0)/kT]$[f]	$1/2\ N_V\exp[-(0.1033-1.1\times10^{-4}T)/kT]$
$V_{Zn}' \Longleftrightarrow V_{Zn}'' + h^{\bullet}$	$K_6 = [V_{Zn}''] p / [V_{Zn}']$	$2N_V\exp[-(>2.0)/kT]$	$2N_V\exp[-(2.892-3.1\times10^{-4}T)/kT]$
$Nil \Longleftrightarrow e' + h^{\bullet}$	$K_i = np$	$N_C N_V\exp(-E_g/kT)$[g]	$N_C N_V\exp(-E_g/kT)$
	m_e*[d]	$0.28m_0$[e]	$0.28m_0$
	m_h*[d]	$0.60m_0$	$0.60m_0$
	$N_C = 2(2\pi m_e^* k/h^2)^{3/2} T^{3/2}$[h]	$7.15\times10^{14} T^{3/2}$	$7.15\times10^{14} T^{3/2}$
	$N_V = 2(2\pi m_h^* k/h^2)^{3/2} T^{3/2}$	$2.24\times10^{15} T^{3/2}$	$2.24\times10^{15} T^{3/2}$
	$E_g = E_g(0) - \beta_g T$	$3.45 - 3.7\times10^{-4} T$	$3.45 - 3.7\times10^{-4} T$

[a] For the defects, Kröger–Vink's notation is used.
[b] p_{O2} and p_{Zn} are the oxygen and zinc partial pressures.
[c] n and p are the electron and hole concentrations.
[d] m_e* and m_h* are the electron and hole effective masses.
[e] m_0 is the free electron mass.
[f] N_C and N_V are the conduction and valence band density of states.
[g] E_g is the band gap energy.
[h] k and h are the Boltzman and Planck constants, respectively.
[i] Note that the units of the constants in Sukker and Tuller's model and in the modified one are the same as those in Kröger's model in Table 2 and, therefore, are omitted.

range. Therefore, in our calculations we will assume that Eq. (2) predominates over Eq. (3). Since we might be in the border line between the two possible mechanisms, we checked the influence of Eq. (3) on the room temperature conductivities, and arrived at the conclusion that the presence of oxygen vacancies in a total amount equal to 10% of the total amount of the zinc interstitials does not affect the room temperature conductivity of the samples. This is because the energy of ionisation of the oxygen vacancy is much higher than the one for the zinc interstitial (see Tables 2 and 3). Since we found that the oxygen vacancies are probably present in the material in a small amount,[27] we assumed in our calculation an oxygen vacancy concentration of 10%.

Using any of the other models proposed in Tables 2 and 3 (rather than the present one) together with the value of $\mu = 100\ cm^2/Vs$, we could not reproduce the conductivity values shown in Fig. 2 (the calculation procedure is shown in the appendix). This means that some of the equilibrium constants should be revised. We annealed the present Mn-doped samples at 1073 K for 2 hours and found that they showed nonlinear current-voltage characteristics.[27] By measuring the admittance spectra of these annealed samples and using the same method as described in Ref. 18, we detected the presence of three loss peaks with energies of ~0.05, ~0.20 and

Table 4
Defect ionisation energies near room temperature for ZnO in the Sukker and Tuller's model and in the present work

Defect	Ionisation energy (eV) (Sukker and Tuller's model)	Ionisation energy (eV) (present work)
$Zn_i^{\bullet}$	0.05	0.05
$Zn_i^{\bullet\bullet}$	0.20	0.20
$V_O^{\bullet}$	0.50	0.32
$V_O^{\bullet\bullet}$	~2.0	2.0
V_{Zn}'	~0.90–1.0	1.0
V_{Zn}''	⩾2.0	2.8

~0.32 eV between 10 and 300 K,[27] in accordance with the reported values for donor-like levels in the band gap of ZnO, ~0.05, ~0.20, ~0.32, ~0.50 and ~2.0 eV, below the conduction band edge.[28–39] The energy depth was restricted to less than 0.50 eV due to the limited frequency and temperature window used in that work.[27] The results about the nonlinear current-voltage characteristics and the admittance spectra of the annealed samples will be published in a forthcoming paper. The 0.05 eV level was also found previously by electrical conductivity measurements,[28] and assigned to the first ionisation of the zinc interstitial. The 0.20 eV level, also found by deep level transient spectroscopy (DLTS),[29–32] admittance spectroscopy (AS),[33–36] and dc conductivity measurements,[28] was assigned to the second ionisation of Zn_i. Finally, the level 0.32 eV, also found by DLTS[29–32] and AS[33–37] was assigned to the first ionisation of the oxygen vancancy, $V_O^{\bullet}$. For the second ionisation of this defect we took the value of 2.0 eV, which was observed by luminescence[38] and cathodoluminescence[39] measurements.

It is generally accepted that the intrinsic acceptors in ZnO are the singly and doubly ionised zinc vacancies (V_{Zn}' and V_{Zn}''). The acceptor energy level of V_{Zn}' has been obtained in the ~0.8–1.1 eV range above the valence band edge, by several optical measurements.[39–41] By analogy to ZnS, the acceptor level of V_{Zn}'' has been estimated to lie ~2.8 eV above the valence band edge.[13] Table 3 shows the values used in the present calculations for the donors and acceptors in ZnO, together with the values for K_{ZnO}, K_O, K_F, and K_S constants. Comparing the values used in the present work with those of the Sukker and Tuller model in Tables 3 and 4, it can be seen that the main difference lies in the second ionisation energy for the oxygen vacancy, 0.32 eV instead of 0.50 eV, and on the temperature dependence of the donors and acceptors energies. We do not know the temperature dependency of those energies, and we have simply assumed that they change with temperature following an equation of the type,[42]

$$E_i = E_{i0} + \beta_i T, \tag{4}$$

where E_{i0} is the ionisation energy at 0 K, and β_i is the temperature coefficient, determined by

$$\beta_i = \beta_g E_{i0}/E_{g0}, \tag{5}$$

where β_g is the temperature coefficient of the band gap, and E_{g0} is the band gap at 0 K. If this type of correction of the donors and acceptors energies is not performed, again the room temperature conductivities calculated from the high temperature equilibrium do not agree with the experimental ones (Fig. 1).

We finally need the energy for the manganese. Mn is normally related to a deep donor in ZnO,[15,18,20–22] with the energy of 0.7 eV,[15] or 0.45–0.50 eV,[18] or ~2.0 eV[20–22] below the conduction band edge. As shown later, our results agree with the last value and, therefore we will use this value in the calculations.

Fig. 3 shows the calculated and the experimental conductivities at room temperature, like in Fig. 1. In spite of the many assumptions made, namely using the same electron mobility value and the variations of the energies with temperature, it can be seen that the agreement between the calculated and the experimental conductivities is very good, particularly noting that the conductivity values change for around seven orders of magnitude. To explain the effect of Mn addition, we present in Fig. 4 the high temperature (sintering temperature) defect concentrations for pure ZnO (Fig. 4a) and for the 0.6 mol% Mn-doped sample (Fig. 4c), and the room temperature defect concentrations for the same samples (Fig. 4b and d, respectively). The 0.1 mol% and the 0.3 mol% Mn-doping give the same qualitative results as the 0.6 mol% case. Fig. 4a shows that at the sintering temperature, the carrier concentrations in pure ZnO is controlled by the zinc interstitial defects, while in Mn-doped samples (Fig. 4c), the carrier concentration is controlled by the high content of the Mn defect. In this case, the concentration of the zinc interstitials is low. If these samples are quenched, at room temperature the carrier concentration is always controlled by the zinc interstitials (the Mn defect can not be ionised due to the high energy required, ~2.0 eV, and stays in the lattice as Mn^{2+}), and, since the concentration of zinc interstitials was depressed at high temperature due to the presence of Mn, the carrier concentration is low in this sample (Fig. 4d), and, therefore, the conductivity is also low (Fig. 3). Therefore, it can be stated that a small amount of Mn, below the solubility limit in ZnO, makes ZnO a resistive material at room temperature because it depresses the concentration of the predominant defect, the zinc interstitials, at the sintering temperature. Ohashi et al.[23] obtained a non-linear behaviour in Mn-doped ZnO bicrystals, but also in Co-doped ZnO and not in

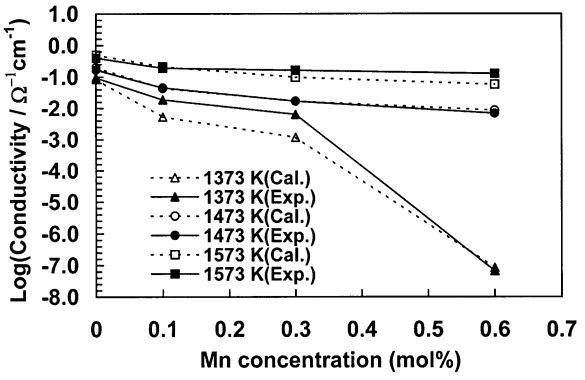

Fig. 3. Calculated and experimental conductivities at 300 K of undoped and Mn-doped ZnO, quenched from 1373, 1473 and 1573 K, respectively.

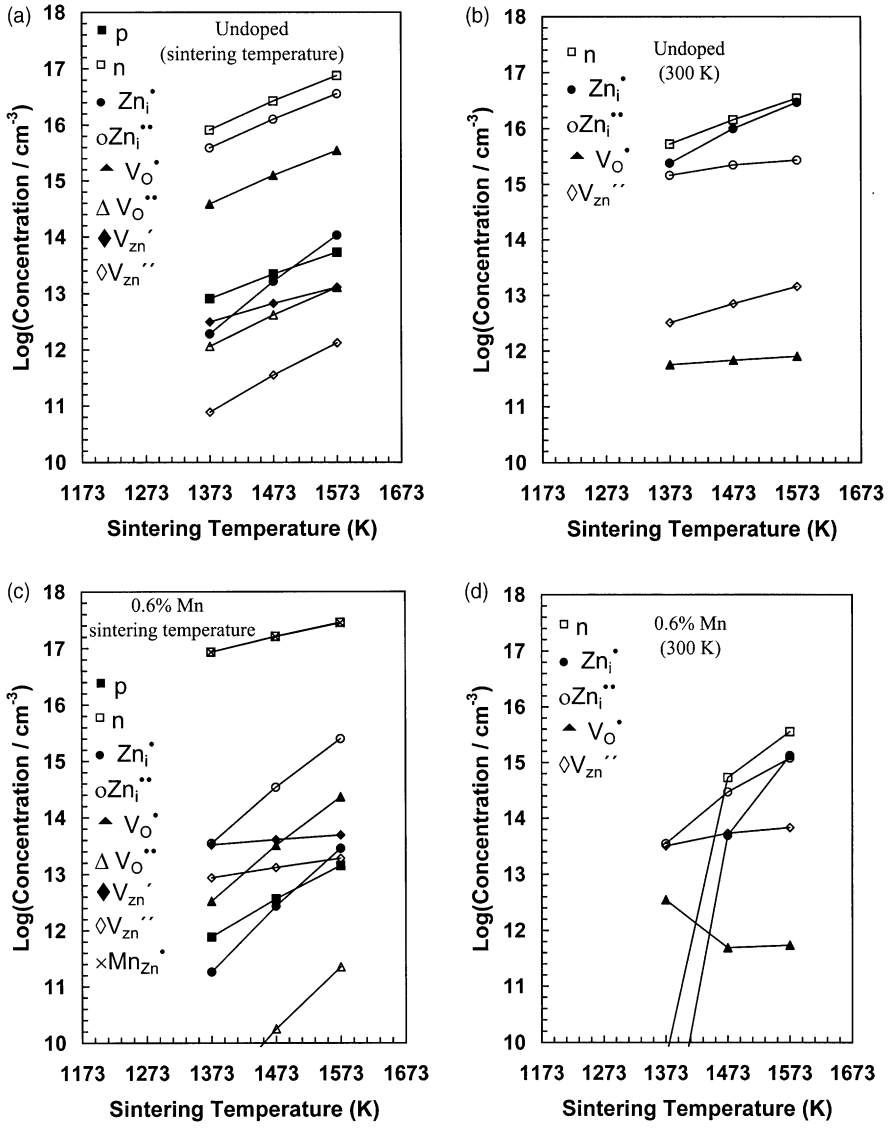

Fig. 4. Defect concentrations in the sintered samples as a function of the sintering temperature: (a) defect concentrations for undoped ZnO at the sintering temperatures, (b) defect concentrations for undoped ZnO at 300 K, quenched from the sintering temperatures, (c) defect concentrations for ZnO doped 0.6 mol% Mn at the sintering temperatures, and (d) defect concentrations for ZnO doped with 0.6 mol% Mn at 300 K, quenched from the sintering temperatures.

undoped ZnO bicrystals. However, they obtained the bicrystals by hot pressing undoped or doped single crystals in an oxygen rich atmosphere, therefore changing the grain boundary status.

A last point to address in this section is the choice of the energy level of the Mn defect. Mn was assumed to be a deep donor with an ionisation energy of ~2.0 eV below the conduction band edge at room temperature. To estimate the energy level of this defect at room temperature, we compared the experimental conductivities of the 0.1, 0.3 and 0.6 mol% Mn samples with those generated by the model we used, by changing the energy level of the defect from 0 to 3.2 eV from the conduction band edge, i.e. within the ZnO band gap. The results are summarised in Fig. 5, and it can be seen that the best agreement is found for an energy of ~2.0 eV. This result perfectly agrees with those found experimentally by optical absorption,[20–22] which further corroborates our model calculations.

3.2. Low temperature behaviour

In the previous section, we have assumed a constant carrier mobility (100 cm^2/Vs) at room temperature for all the samples, whatever the sintering temperature or the composition of the samples. Now, it must be further analysed. In this section, we will analyse the temperature dependence of the mobility for the samples of different compositions quenched from different sintering temperatures. To do this, the carrier concentrations, n_{cal}, at lower temperatures, from 70 to 300 K, were calculated using the proposed procedure in the former section.

Then the values for the mobility, $\mu = \sigma_{exp}/en_{cal}$, at lower temperatures were obtained by using the calculated carrier concentrations, n_{cal}, and the experimental conductivities, σ_{exp}. It must be emphasised at this point, the basic procedure we took in this paper. We firstly compared the experimental conductivities of the quenched samples with those calculated from the defect chemistry model (giving the carrier concentration, n) and an assumption of a constant but reasonable value for the carrier mobility ($\mu = 100$ cm^2/Vs) in ZnO. Due to the general and good agreement between the two, we could assume the validity of the defect model for the system, and now we can access the mobilities at different temperatures, for the various compositions, knowing the conductivities (experimental) and the carrier concentrations (calculated). In doing this, we can further validate the used defect model if these calculated mobilities agree with the reported ones for ZnO, and also further improve the knowledgement of the role of Mn in the electrical properties of ZnO.

Fig. 6 shows the calculated electron mobilities, $\mu = \sigma_{exp}/en_{cal}$, in the temperature range of 70–300 K for undoped samples sintered at different temperature and for the 1473 K sintering samples with different Mn content. For undoped ZnO, with decreasing the temperature, the mobility increases in the higher temperature range, 300–170 K, and then decreases in the lower one, 140–70 K. This indicates that phonon scattering dominates the electron mobility at the higher temperature range, and ionic defect scattering is predominant at the lower temperature range. Similar temperature dependence for the electron mobility in ZnO single crystals was observed in Refs. 23 and 25. The value of the mobility of undoped

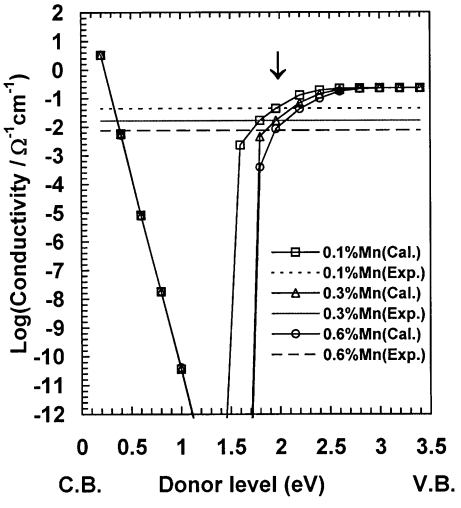

Fig. 5. Calculated conductivities at 300 K for Mn-doped ZnO, quenched from 1473 K as a function of the Mn energy level below the conduction band edge, and comparison with the experimental conductivity values. C.B. and V.B. mean conduction band and valence band, respectively. The arrow indicates the best agreement between the calculated and the experimental conductivities.

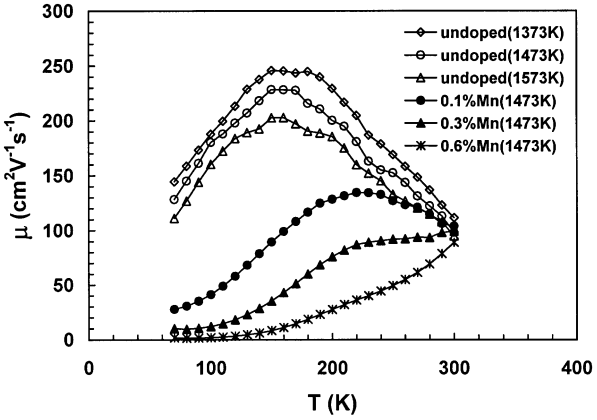

Fig. 6. Calculated electron mobilities at temperatures between 70 and 300 K for undoped samples sintered at different temperatures, and for 1473 K sintering samples with different Mn contents.

ZnO in Fig. 6 (around 100–250 cm^2/Vs at 70–300 K) is also in general agreement with the value in Ref. 25 (around 70–200 cm^2/Vs at 70–300 K, in samples heated at 1473 and 1593 K, respectively), and in Ref. 23 (around 150–300 cm^2/Vs at 83–300 K, in samples annealed at 1073–1273 K). The mobility of undoped ZnO decreases with the increase in the sintering temperature, and this can be due to the increase in the ionised donor concentrations, as shown in Fig. 4, thus increasing the ionic defect scattering. This effect of the ionised donor concentration was also observed in Ref. 23. In the case of Mn-doping, the mobility significantly decreases upon its addition to the material, and the higher the Mn concentration, the lower the mobility. This could be explained by an impurity scattering process due to the very high concentration ($> 10^{19}$ cm^{-3}) of Mn in the materials. However, care should be put in this case because the mobilities at low temperatures are very low and there is the possibility that the conduction process is dominated by a hopping mechanism in this temperature range. Some more experimental work on the determination of the mobility in these samples must be carried on, which is out of the scope of the present work. Results will be published in a forthcoming paper.

4. Conclusions

Samples of undoped ZnO and ZnO doped with Mn from 0.1 to 0.6 mol% were sintered at 1373, 1473 and 1573 K, for 2 h, in air, and then quenched to room temperature. Defect equilibria and electrical characteristics of these samples were studied for the sintering temperatures, and for room temperature and below, respectively. From these studies, it was possible to assume that the presence of oxygen vacancies is negligible in the defect equilibria in ZnO under the present experimental conditions, and we found that the temperature dependence of the ionisation energies of the defects in ZnO significantly

affects the defect equilibria at different temperatures. Hence, not only the temperature coefficient of the band gap but also the temperature coefficients of the ionisation energies of the defects must be taken into account for the calculations of the defect equilibria.

Defect concentrations in undoped and Mn-doped ZnO at the sintering temperatures and at room temperature and below were calculated, and the calculated results show that Mn doping with high concentration enhances the electron concentration at high temperatures, but depresses it at room temperature. Using the calculated electron concentrations and assuming a constant electron mobility of 100 cm^2/Vs, the conductivities at room temperature were calculated and compared with the experimental ones. The agreement between the experimental and calculated conductivities was very good for all the samples of undoped and Mn-doped ZnO. In Mn-doped ZnO, the energy level of Mn donor in ZnO was estimated to be at $\sim$2.0 eV below the conduction band edge. Using the experimental conductivities and the calculated electron concentrations, the electron mobilities were calculated between 70 and 300 K. The result shows that the temperature dependence of the mobility in undoped ZnO is similar to that in ZnO single crystals observed in other works, and Mn-doping in this work significantly reduces the electron mobility below room temperature, probably by an impurity scattering process due to the very high concentration ($> 10^{19}\,cm^{-3}$) of Mn in the materials. The role of Mn on the electrical conductivity of ZnO could then be understood: it makes ZnO highly conductive at high temperature, where $n \approx [Mn_{Zn}^{\bullet}]$, and resistive at room temperature, with the resistivity depending on the Mn concentration and on the sintering temperature.

Acknowledgements

The author J.H would like to thank the Praxis XXI programme of the Foundation for Science and Technology (FCT), Portugal for financial support.

Appendix

The procedure for the calculation of the defect concentrations in undoped and Mn-doped ZnO at the sintering temperatures, and at room temperature and below is in the following.

(1) Defect concentrations at the sintering temperatures. Keeping the samples of undoped and Mn-doped ZnO at the high sintering temperatures, the chemical balance between the species $Zn_i^{\times}$, $Zn_i^{\bullet}$, $Zn_i^{\bullet\bullet}$, $V_O^{\times}$, $V_O^{\bullet}$, $V_O^{\bullet\bullet}$, $V_{Zn}^{\times}$, V_{Zn}', V_{Zn}'', $Mn_{Zn}^{\times}$, $Mn_{Zn}^{\bullet}$, e', and $h^{\bullet}$, is maintained according to the reactions shown in Table 3 and the reactions (1a)–(4a) shown below.

Since manganese acts as a donor in ZnO, the following defect reaction must be added to the defect model,

$$Mn_{Zn}^{\times} \iff Mn_{Zn}^{\bullet} + e', \tag{1a}$$

where we are assuming a substitutional solid solution in the cation site. Its corresponding mass action is

$$K_{Mn} = [Mn_{Zn}^{\bullet}]n/[Mn_{Zn}^{\times}] = 2N_C\exp(-E_{M_n}/kT), \tag{2a}$$

with E_{Mn} being the ionisation energy for the Mn donor. The total donor concentration, $[Mn_{Zn}]$, is, therefore,

$$[Mn_{Zn}] = [Mn_{Zn}^{\times}] + [Mn_{Zn}^{\bullet}]. \tag{3a}$$

From Eqs. (2a) and (3a), it can be derived that

$$[Mn_{Zn}^{\bullet}] = K_{Mn}[Mn_{Zn}]/(K_{Mn} + n). \tag{4a}$$

For undoped ZnO, the electroneutrality condition is

$$n + [V_{Zn}'] + 2[V_{Zn}''] = p + [Zn_i^{\bullet}] + 2[Zn_i^{\bullet\bullet}] + [V_O^{\bullet}] + 2[V_O^{\bullet\bullet}]. \tag{5a}$$

At the sintering temperature, the mass action for the ionic defects holds. In the case of the oxygen vacancy, one has

$$[V_O]_{Total} = [V_O^{\times}] + [V_O^{\bullet}] + [V_O^{\bullet\bullet}]. \tag{6a}$$

As discussed above, a reasonable amount for the oxygen vacancy is 10% of the total zinc interstitial concentration,

$$[V_O]_{Total} = 0.1[Zn_i]_{Total} = 0.1([Zn_i^{\times}] + [Zn_i^{\bullet}] + [Zn_i^{\bullet\bullet}]). \tag{7a}$$

Taking the equations of the mass actions in Table 3 together with Eq. (6a) and the assumption shown in Eq. (7a), one obtains for the electroneutrality condition,

$$\begin{aligned} &n + K_5K_Op_{O2}^{1/2}n/K_i + 2K_6K_5K_Op_{O2}^{1/2}n^2/K_i^2 \\ &= K_i/n + K_1K_Rp_{O2}^{-1/2}/n + 2K_2K_1K_R{p_{O2}}^{-1/2}/n^2 \\ &+ (K_3/n)(1 + K_3/n + K_3K_4/n^2)^{-1} \\ &0.1(K_Rp_{O2}^{-1/2} + K_1K_R{p_{O2}}^{-1/2}/n + 2K_2K_1K_R{p_{O2}}^{-1/2}/n^2) \\ &+ 2(K_4K_3/n^2)(1 + K_3/n + K_3K_4/n^2)^{-1} \\ &0.1(K_Rp_{O2}^{-1/2} + K_1K_R{p_{O2}}^{-1/2}/n + 2K_2K_1K_R{p_{O2}}^{-1/2}/n^2). \end{aligned} \tag{8a}$$

Keeping the samples at the chosen sintering temperatures, 1373, 1473 and 1573 K in air, and with $p_{O2} = 0.2$

atm, the concentration of electrons, n, can be obtained by numerically solving Eq. (8a). Then, one can obtain the other defect concentrations.

In the case of Mn-doped ZnO, the electroneutrality condition is now

$$n + [V'_{Zn}] + 2[V''_{Zn}] = p + [Zn_i^{\bullet}] + 2[Zn_i^{\bullet\bullet}] + [V_O^{\bullet}] + 2[V_O^{\bullet\bullet}] + [Mn_{Zn}^{\bullet}]. \quad (9a)$$

Using the same procedure as before, one obtains

$$\begin{aligned} &n + K_5 K_O {p_{O2}}^{1/2} n/K_i + 2K_6 K_5 K_O p_{O2}{}^{1/2} n^2/K_i^2 \\ &= K_i/n + K_1 K_R p_{O2}{}^{-1/2}/n + 2K_2 K_1 K_R p_{O2}{}^{-1/2}/n^2 \\ &+ (K_3/n)(1 + K_3/n + K_3K_4/n^2)^{-1} \\ &0.1(K_R p_{O2}^{-1/2} + K_1 K_R p_{O2}{}^{-1/2}/n + 2K_2 K_1 K_R p_{O_2}{}^{-1/2}/n^2) \\ &+ 2(K_4K_3/n^2)(1 + K_3/n + K_3K_4/n^2)^{-1} \\ &0.1(K_R p_{O2}^{-1/2} + K_1 K_R p_{O2}{}^{-1/2}/n + 2K_2 K_1 K_R p_{O2}{}^{-1/2}/n^2) \\ &+ K_{Mn}[Mn_{Zn}]/(K_{Mn} + n). \end{aligned} \quad (10a)$$

Since in the present work $[Mn_{Zn}]$ is assumed to be equal to the doping level of Mn in ZnO, which is a known quantity, Eq. (10a) can also be numerically solved to obtain n. Then, again, the other defect concentrations can be found.

(2) Defect concentrations at room temperature and below. After reaching equilibrium at the high sintering temperatures, samples were quenched to room temperature. The total high temperature equilibrium concentrations of the ionic defects are considered to be frozen in the materials, due to the fast cooling and negligible diffusion of the ions or vacancies, whereas a new electronic equilibrium can be established since electrons and holes diffuse rapidly at low temperatures. Therefore, the total concentrations of the defects Zn_i, V_O, and V_{Zn}, remain unchanged, while the relative amount of the charge state of each defect will change with temperature.

For undoped ZnO at room temperature and below, the electroneutrality condition of Eq. (5a) still holds, and becomes

$$\begin{aligned} &n + (K_5 n/K_i + 2K_6K_5n^2/K_i^2) \\ &(1 + K_5 n/K_i + K_5K_6n^2/K_i^2)^{-1} \\ &[V_{Zn}]_{Total} = K_i/n + (K_1/n + 2K_2K_1/n^2) \\ &(1 + K_1/n + K_1K_2/n^2)^{-1} \\ &[Zn_i]_{Total} + (K_3/n + 2K_4K_3/n^2) \\ &(1 + K_3/n + K_3K_4/n^2)^{-1}\ [V_O]_{Total}. \end{aligned} \quad (11a)$$

Since $[V_{Zn}]_{Total}$, $[Zn_i]_{Total}$, and $[V_O]_{Total}$ can be obtained from the calculations for the sintering temperatures, Eq. (11a) can be numerically solved to obtain the value of n, then the other defect concentrations can be found.

Similarly, for Mn-doped ZnO at room temperature and below, the electroneutrality condition of Eq. (9a) still holds and can be transformed to

$$\begin{aligned} &n + (K_5 n/K_i + 2K_6K_5n^2/K_i^2) \\ &(1 + K_5 n/K_i + K_5K_6n^2/K_i^2)^{-1}[V_{Zn}]_{Total} \\ &= K_i/n + (K_1/n + 2K_2K_1/n^2) \\ &(1 + K_1/n + K_1K_2/n^2)^{-1}[Zn_i]_{Total} \\ &+ (K_3/n + 2K_4K_3/n^2) \\ &(1 + K_3/n + K_3K_4/n^2)^{-1}[V_O]_{Total} \\ &+ K_{Mn}[Mn_{Zn}]/(K_{Mn} + n) \end{aligned} \quad (12a)$$

After numerically solving for n, the other defect concentrations can be found.

References

1. Gupta, T. K., Application of zinc oxide varistors. *J. Am. Ceram. Soc.*, 1990, **73**, 1817–1840.
2. Costa, M. E. V., Mantas, P. Q. and Baptista, J. L., Effect of electrode alterations on the a.c. behaviour of Li_2O–ZnO humidity sensors. *Sens. Actuators*, 1995, **B26–27**, 312–314.
3. Shiosaki, T. and Kawabata, A., Piezoelectric thin films for SAW applications. *Ferroelectrics*, 1982, **42**, 219–232.
4. Dutta, S., Jackson, H. E., Boyd, J. T., Hickernell, F. S. and Davis, R. L., Scatter loss reduction in ZnO optical waveguides by laser annealing. *Appl. Phys. Lett.*, 1981, **39**, 206–208.
5. Horsthuis, W. H. G., ZnO processing for integrated optic sensors. *Thin Solid Films*, 1986, **137**, 185–192.
6. Mantas, P. Q. and Baptista, J. L., The barrier height formation in ZnO varistor. *J. Eur. Ceram. Soc.*, 1995, **15**, 605–615.
7. Baptista, J. L. and Mantas, P. Q., High temperature characterisation of electrical barriers in ZnO varistors. *J. Electroceram.*, 2000, **4**, 215–224.
8. Mantas, P. Q., Senos, A. M. R. and Baptista, J. L., Varistor-capacitor characteristics of ZnO ceramics. *J. Mater. Sci.*, 1986, **21**, 679–686.
9. Baptista, J. L., Mantas, P. Q. and Frade, J. R., Grain boundary induced perturbation in electrical ceramics. In *Ceramic Transactions, Vol. 71*, ed. K. Kuomoto, L. M. Sheppard and H. Matsubara. American Ceramic Society, OH, 1996, pp. 61–77.
10. Hagemark, K. I., Defect structure of Zn-doped ZnO. *J. Solid State Chem.*, 1976, **16**, 293–299.
11. Secco, E. A. and Moore, W. J., Diffusion and exchange of zinc in crystalline zinc oxide. *J. Chem. Phys.*, 1957, **26**, 942–948.
12. Sukker, M. H. and Tuller, H. L., Defect equilibria in ZnO varistor materials. In *Advances in Ceramics*, Vol. 7, *Additives and Interfaces in Electronic Ceramics*, ed. M. F. Yan and A. H. Heuer, American Ceramic Society, OH, 1983, pp. 71–90.
13. Kröger, F. A., *The Chemistry of Imperfect Crystals, Vol. 2*. North-Holland, Amsterdam, 1974 pp. 743–752..
14. Mahan, G. D., Intrinsic defects in ZnO varistors. *J. Appl. Phys.*, 1983, **54**, 3825–3832.
15. Einzinger, R., Grain boundary phenomena in ZnO varistors. In *Grain Boundaries in Semiconductors, Mater. Res. Soc. Symp. Proc.* ed. H. J. Leamy, G. E. Pike and C. H. Seager. Elsevier, New York, 1982, pp. 343–355.

16. Han, J., Senos, A. M. R. and Mantas, P. Q., Nonisothermal sintering of Mn-doped ZnO. *J. Eur. Ceram. Soc.*, 1999, **19**, 1003–1006.
17. Han, J., Mantas, P. Q. and Senos, A. M. R., Grain growth in Mn-doped ZnO. *J. Eur. Ceram. Soc.*, 2000, **20**, 2753–2758.
18. Greuter, F. and Blatter, G., Electrical properties of grain boundaries in polycrystalline compound semiconductors. *Semicond. Sci. Technol.*, 1990, **5**, 111–137.
19. Sukkar, M. H. and Tuller, H. L., ZnO interface electrical properties-role of oxygen chemisorption. In *Non-toichiometric Compounds: Surfaces, Grain Boundaries and Structural Defects*, ed. J. Nowtny and W. Weppner. Kluwer, Dordrecht, 1989, pp. 237–263.
20. Kleinlein, F. W. and Helbig, R., Diffusion constant and typical near-band edge absorption of manganese in zinc oxide crystals. *Z. Phys.*, 1974, **266**, 201–207.
21. Jakani, M., Campet, G., Claviere, J., Fichou, D., Pouliquen, J. and Kossanyi, J., Photoelectrochemical properties of zinc oxide doped with 3d elements. *J. Solid State Chem.*, 1985, **56**, 269–277.
22. Fichou, D., Pouliquen, J., Kossanyi, J., Jakani, M., Campet, G. and Claviere, J., Extension of the photoresponse of semiconducting zinc oxide electrodes by 3d-impurities absorbing in the visible region of the solar spectrum. *J. Electroanal. Chem.*, 1985, **188**, 167–187.
23. Ohashi, N., Terada, Y., Ohgaki, T., Tanaka, S., Tsurumi, T., Fukunaga, O., Haneda, H. and Tanaka, J., Synthesis of ZnO bicrystals doped with Co or Mn and their electrical properties. *Jpn. J. Appl. Phys.*, 1999, **38**, 5028–5032.
24. Clarke, D. R., Varistor ceramics. *J. Am. Ceram. Soc.*, 1999, **82**, 485–502.
25. *Physik der II-VI und I-VII-Verbindungen, semimagnetische Halbleiter*, Landolt-Börnstein, new series, III/17b, ed. O. Madelung, Springer-Verlag, Berlin, 1982, p. 346.
26. Senos, A. M. R., *Sintering kinetics in open porosity stages of zinc oxide.*, PhD thesis, University of Aveiro, Aveiro, Portugal, 1993.
27. Han, J., Mantas, P. Q., Senos, A. M. R., unpublished data.
28. Hagemark, K. I. and Chacka, L. C., Electrical transport properties of Zn-doped ZnO. *J. Solid State Chem.*, 1975, **15**, 261–270.
29. Tsuda, K. and Mukae, K., Characterization of the interface state in ZnO varistors by DLTS methods. *Jpn. J. Ceram. Soc.*, 1989, **97**, 1211–1218.
30. Rohatgi, A., Pang, S. K., Gupta, T. K. and Straub, W. D., The deep level transient spectroscopy studies of a varistors as a function of annealing. *J. Appl. Phys.*, 1988, **63**, 5375–5379.
31. Shohata, N., Matsumura, T. and Ohno, T., DLTS measurement on non-ohmic zinc oxide ceramic varistors. *Jpn. J. Appl. Phys.*, 1980, **19**, 1973–1974.
32. Nitayama, A., Sakaki, H. and Ikoma, T., Properties of deep level in ZnO varistors and their effect on current-response characteristics. *Jpn. J. Appl. Phys.*, 1980, **19**, 1743–1746.
33. Cordaro, J. F., Shim, Y. and May, J. E., Bulk electron traps in zinc oxide varistors. *J. Appl. Phys.*, 1986, **60**, 4186–4190.
34. Greuter, F., Blatter, G., Rossinelli, M. and Stucki, F., Conduction mechanism in ZnO varistors: an overview. In *Ceramic Transactions, Vol. 3: Advances in Varistor Technology*, ed. L. M. Levinson. American Ceramic Society, OH, 1989, pp. 31–53.
35. Rossinelli, M., Blatter, G. and Greuter, F., Grain boundary properties of ZnO varistors. In *Electrical Ceramics*, ed. B. C. H. Steele. British Ceramic Society, Stoke-on-Trent, 1985, pp. 1–17.
36. Alim, M. A., Seitz, M. A. and Hirthe, R. W., Complex plane analysis of trapping phenomena in zinc oxide based varistor grain boundaries. *J. Appl. Phys.*, 1988, **63**, 2337–2345.
37. Shim, Y. and Cordaro, J. F., Admittance spectroscopy of polycrystalline ZnO–Bi_2O_3 and ZnO–BaO systems. *J. Am. Ceram. Soc.*, 1988, **71**, 184–188.
38. Nikitenko, V. A. and Pas'ko, P. G., Thermodynamic analysis of intrinsic defects in single crystals of zinc oxide with deviations from stoichiometry. *Izv. Akad. Nauk. SSSR, Neorg. Mater.*, 1977, **13**, 2026–2030.
39. Bylander, E. G., Surface effects on the low-energy cathodoluminescence of zinc oxide. *J. Appl. Phys.*, 1978, **49**, 1188–1195.
40. Bhushan, S., Pandey, A. N. and Kaza, B. R., Photo and electroluminescence of undoped and rare earth doped ZnO electroluminors. *J. Lumin.*, 1979, **20**, 29–38.
41. Seitz, M. A., Pinter, W. F. and Hirthe, W. H., Thermoluminescence of ZnO. *Mater. Res. Bull.*, 1971, **6**, 275–282.
42. Schwing, U. and Hoffmann, B., Model experiments describing the microcontact of ZnO varistors. *J. Appl. Phys.*, 1985, **57**, 5372–5379.